(Preprint) AAS 16-425

CONSTRUCTION AND VERIFICATION OF A SOLUTION OF THE 8TH GLOBAL TRAJECTORY OPTIMIZATION COMPETITION PROBLEM. TEAM 13: GLASGOWJENA+

Alessandro Peloni,[*] Dietmar Wolz,[†] Matteo Ceriotti,[‡] and Ingo Althöfer [§]

This paper describes the methodology to find and verify the solution to the 8th Global Trajectory Optimization Competition (GTOC) problem, developed by Team 13, GlasgowJena+. We chose a stochastic approach to quickly assess a large number (about 10^{10}) of 3-spacecraft formations. A threshold was used to select promising solutions for further optimization. Our search algorithm (implemented in Java) is based on three C++ algorithms called via Java native interface (JNI). A great deal was given to the verification process, which became a core part of our solution. Our final solution has a performance index of $J = 5.97 \times 10^7$ km, 40 distinct observations, and the sum of the final masses of the three spacecraft is 5846.57 kg.

INTRODUCTION

The problem proposed by Petropoulos for the 8th edition of the Global Trajectory Optimization Competition (GTOC) consists in a high-resolution mapping of radio sources in the universe using space-based Very-Long-Baseline Interferometry. For this purpose, a high-resolution observation of a source is obtained when the perpendicular of the triangle formed by three satellites in Earth orbit is parallel to the direction of the desired radio source. The performance index *J* of the competition depends on the direction of the observed sources and the dimension of the three-spacecraft formation, and is given by

$$J = \sum_{\text{all observations}} Ph\left(0.2 + \cos^2 \delta\right) \tag{1}$$

The term *h* in Eq. (1) refers to the smallest of the three altitudes of the observing triangle, *P* is a weighting factor for repeated observations of the same source, and δ is the declination of the source. For a detailed explanation of the problem at hand we refer to Petropoulos [1].

Since low-declination sources are more valuable, as delineated by Eq. (1), it is firstly important to study the distribution of the sources. Since the radio sources are (approximately) heterogeneously

[*] Ph.D. candidate, School of Engineering, University of Glasgow, Glasgow G12 8QQ, United Kingdom.
[†] Ph.D., Institut für Mathematik, Fakultät für Mathematik und Informatik, Friedrich-Schiller-Universität Jena, 07743 Jena, Germany.
[‡] Lecturer, School of Engineering, University of Glasgow, Glasgow G12 8QQ, United Kingdom.
[§§] Professor, Institut für Mathematik, Fakultät für Mathematik und Informatik, Friedrich-Schiller-Universität Jena, 07743 Jena, Germany.

distributed along the zero-declination belt (see Figure 1), no defined rule can be applied to a source-hunting strategy in order to prioritize the sources with lower declinations.

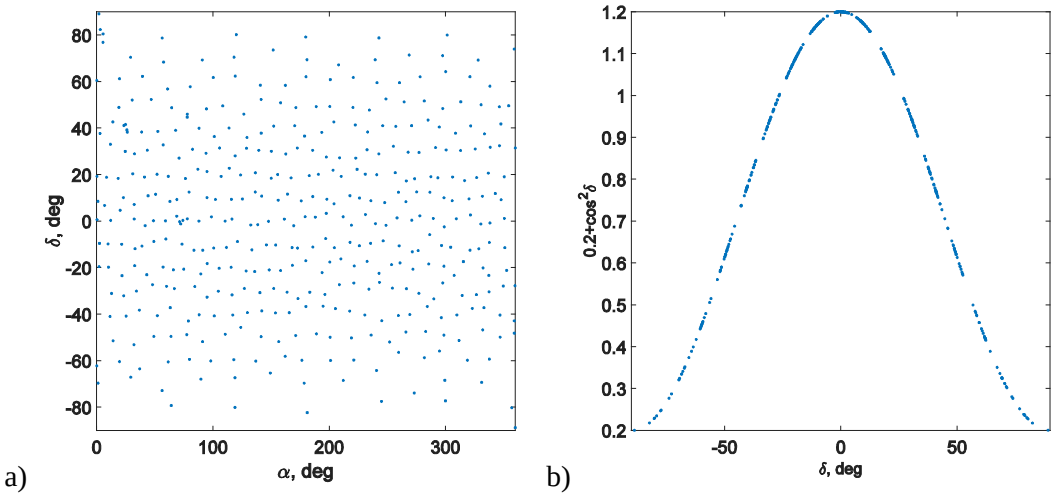

Figure 1. Distribution of the radio sources in the α–δ space (a). Weights of the radio sources as function of the declination (b).

A second peculiarity of this GTOC is the different approach to the trajectory-optimization problem. It is a common approach of space-trajectory problems [2-6], as well as in some of the previous editions of the competition (e.g. GTOC5 [7] and GTOC7 [8]), to target the orbit in a first approximation, and then the phase is adjusted to rendezvous with the actual body on the orbit. In this case instead we cannot target an orbit, as we need to target three points in space, and thus a plane, to observe a source. The orbits of the three spacecraft do not actually matter for the purpose of the single observation. The added challenge is that it is difficult to change the point along the orbit (i.e. the angular position of the spacecraft) in the short period, with a maneuver. It is important to note the fundamental difference between "orbit" and point along the orbit. Orbits (i.e. ellipses) can be changed instantaneously with maneuvers. The position on the orbit is the only function of time, and it can hardly be changed instantaneously with a maneuver. To do so, we need to change the orbit and/or wait for some time.

The general idea of the methodology adopted can be summarized in the following steps:

1. Start from the Earth with one impulsive Δv for each spacecraft, in order to inject it into an orbit towards the Moon.
2. A gravity assist (GA) maneuver at the Moon then changes inclination and/or semi-major axis of each spacecraft's orbit.
3. The three orbits after the Moon swing-by are such that, in the long term, the formation can scan most of the $\alpha-\delta$ space.

The paper is divided into three main sections. The first section contains the description of the methodology used. An important part of this section is dedicated to the description of the verification phase, which turned out to be fundamental for the final results. A second section contains the description of the best solution found, while in the last section conclusions and final remarks are drawn.

DESCRIPTION OF THE METHODOLOGY

A preliminary search of the solution space was performed considering the possible orbits following a Lunar GA at the line of the nodes, and this trajectory propagated in time keeping the 5 slow Keplerian elements $[a, e, i, \Omega, \omega]$ fixed. An optimization through a Particle Swarm Optimizer (PSO) selected triplets of orbits that maximized an approximated final score *J*' within the following assumptions.

1. No constraint on the minimum time between two consecutive "hits"
2. Pointing angle error $\delta\psi \leq 1$ deg
3. Keplerian orbits propagated by means of the algorithm described by Vallado[9] for 6 months with a time step of 0.1 days
4. $P = 1$ always, but only the first 5 "hits" for each source are taken into account, so that it is possible to discard up to two "hits" of the same source if a further optimization is not able to meet any of the constraints

The so-generated triplets of orbits were intended to be used as initial-guess solution for a further optimization that uses the actual available thrust to enforce all the constraints while maximizing the score *J*. However, soon we realized that even minor changes of these orbits through the low thrust could lead to large changes in the targeting of the following sources. As an example, Figure 2 shows the perpendicular path of 10 random highly-inclined formations propagated for about 700 days with no thrust. On the other hand, Figure 3 shows the perpendicular path resulted from a search starting from the initial formations of Figure 2, by applying thrust approximated as 1 deep-space maneuver (DSM). The dots in the figures represent the position of some of the sources in the $\alpha - \delta$ space. For this reason, the following method was followed.

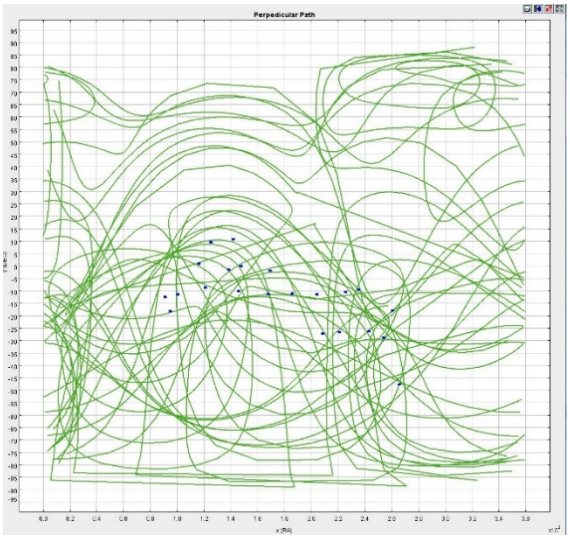

Figure 2. Perpendicular path of 10 random high-inclined formations propagated with no thrust.

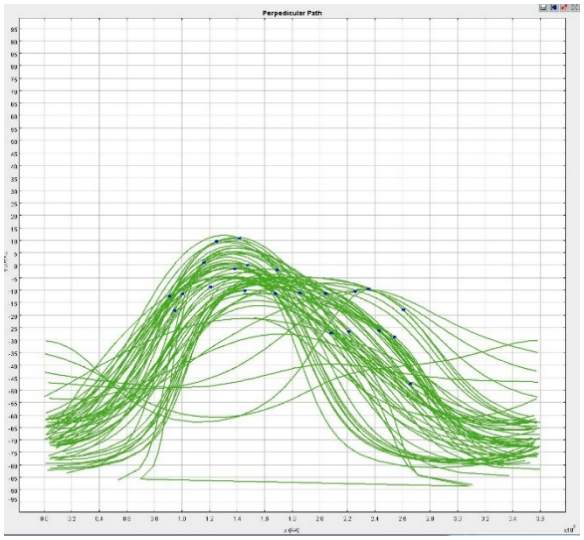

Figure 3. Perpendicular path of 10 random high-inclined formations after applying thrust.

Overall strategy

The overall strategy is: all ships head towards the two nodes of the Moon orbit, where the GA is performed, with the highest possible incoming v_∞, so that we gain the most from the GA maneuvers. In this phase we make no attempt to score, since anyway we could reach only low-valued sources with low *h*. After the GA, time is much more valuable and so we try to reach the Moon as fast as possible using the full 3 km/s impulse at start. After the GA, we proceed by exploring the search space through a beam search handling formations of three spacecraft, as explained in detail in the following sub-sections.

Our search algorithm (implemented in Java) is based on three C++ algorithms called via Java native interface (JNI):

- As a starting point of our development we used the Lambert problem solver described by Izzo[10] and implemented as part of the PyKEP C++ library[*]. Using it we can approximate low-thrust trajectories using our 2-DSM approach very efficiently during search.
- The Taylor propagator[†] was used for the continuous-thrust conversion, with both logarithmic tolerances set to -13.
- Bound Optimization BY Quadratic Approximation (BOBYQA) [11] was used for matching the perpendicular with the targeted sources during search.
- We used code from the Dlib C++ Library[‡].
- CMA-ES[§] is used for continuous-thrust conversion, for the generation of approximated trajectories to the Moon, and for fixing the phasing at the start of the mission. We use the active CMA variant [12] with mirrored sampling [13]. We developed our CMA-ES C++ code from our contribution to Apache Commons Math[**].
- As a starting point of our development we used the Orekit library[††] which is currently mainly used for verification purposes.
- MATLAB was mainly used for verification purposes. Moreover, initial formations after Moon GA have been evaluated through a PSO developed in MATLAB [14].

Gravity Assists of the Moon

Although we performed experiments with 2 GAs per spacecraft, their complexity and the restricted time prevented us to use them. We restricted the encounter of the Moon at its orbital nodes mainly because of the high cost of a plane change, needed to reach the Moon out of the plane. In addition, by omitting the third dimension, the complexity/dimensionality of the optimizations used is largely reduced.

In a first attempt we used a preliminary 3.1 km/s impulse from the initial orbit to generate transfers to the Moon, since an impulse of at least 3.09 km/s is needed to reach the Moon from the starting circular 400 km orbit. This way we could generate formations produced by random GAs which were pre-evaluated by analyzing the path of their perpendicular over time without applying

---

[*] "PyKEP scientific library", URL: http://esa.github.io/pykep/, accessed on Jan, 6th 2016.
[†] ESA. *Taylor propagator source code*. URL: https://github.com/esa/pykep/blob/master/src/core_functions/propagate_taylor.h, accessed on Jan, 6th 2016.
[‡] "Dlib C++ library (optimization)", URL: http://dlib.net/optimization.html, accessed on Jan, 6th 2016.
[§] "CMA-ES source code", URL: https://www.lri.fr/~hansen/cmaes_inmatlab.html, accessed on Jan, 6th 2016.
[**] "Class CMAESOptimizer", URL: https://commons.apache.org/proper/commons-math/javadocs/api-3.1/org/apache/commons/math3/optim/nonlinear/scalar/noderiv/CMAESOptimizer.html, accessed on Jan, 6th 2016.
[††] "Orekit", URL: https://www.orekit.org/, accessed on Jan, 6th 2016.

thrust. Following the method presented by Ceriotti and McInnes[15], in fact, the outgoing orbit after the Moon GA depends only on the flight path angle (γ) and the radius at pericenter of Moon GA (r_P). Figure 4 to Figure 6 show all the possible orbits after encountering the Moon at its ascending node. The angle γ, which belongs to the interval $[0, 2\pi]$, has been sampled in 20 equally-spaced points; the radius of pericenter of the Moon GA has been sampled in 20 logarithmic-spaced points in the interval $r_p \in \left[R_{Moon} + 50,\ R_{Moon} + 5\times10^5 \right]$ km. The choice of the logarithmic-spaced points has been driven by the fact that trajectories close to the Moon are more sensitive to the parameters.

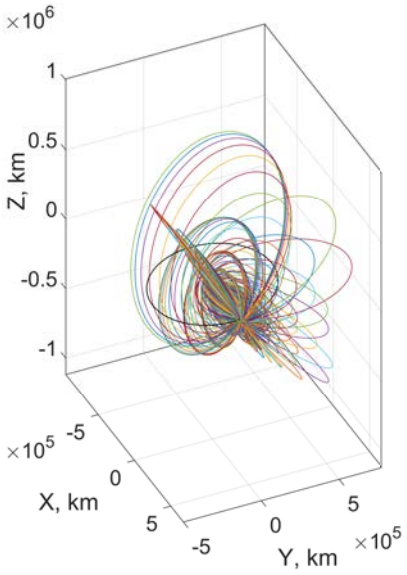

Figure 4. All possible orbits after Moon GA

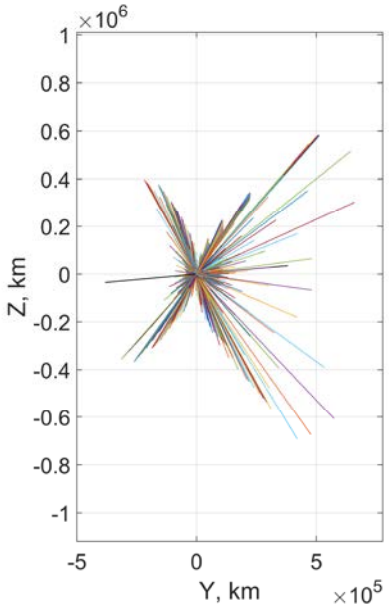

Figure 5. All possible orbits after Moon GA (Y-Z view)

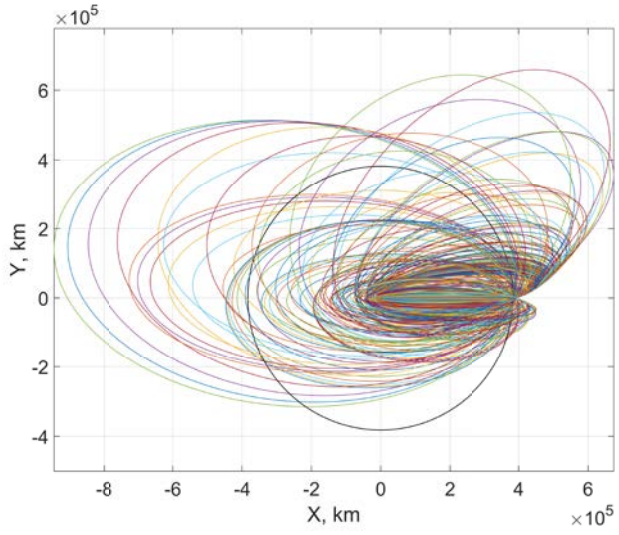

Figure 6. All possible orbits after Moon GA (X-Y view)

From the Earth to the Moon

Now we analyzed how to reach the Moon orbit nodes with the required initial impulse of only 3 km/s. Preliminary calculations based on search results for different starting formations after GA showed us that high incoming v_∞ at the Moon is very desirable and that it is probably worth to extend the time of flight to the Moon to achieve this. We followed the impulse at the Earth with a low-thrust transfer to increase the v_∞ at the Moon. The low-thrust transfers are both based on analytical methods and alternatively through a numerical optimization to raise the apogee. Since we fly with zero inclination and always use full thrust (bang-bang control), the local optimization problems are 1-dimensional and efficiently solvable. We stored many of these flight paths to the Moon nodes and used them (and their incoming v_∞) as basis for the generation of random formations after the GA.

Analytical law to raise the apogee. The analytical law to raise the apogee is based on the instantaneous rate of change of the osculating radius of apogee. By using the Lagrange's variational equations in Gauss' form [16], the instantaneous rate of change of the apogee $\dot{r}_a$ is given by

$$\dot{r}_a = 2a\left[\frac{av}{\mu}(1+e)+\frac{e+\cos\vartheta}{v}\right]f_t - \frac{r}{v}\sin\vartheta\, f_n \tag{2}$$

where $\left[a,e,i,\Omega,\omega,\vartheta\right]^T$ is the set of conventional Keplerian elements and r,v are the magnitude of position and velocity, respectively. f_t, f_n are the force per unit mass (i.e. acceleration) in the tangential and normal direction, respectively. Since this is a two-dimensional problem, the acceleration can be described through the thrust angle ϕ, defined as the angle between the tangential direction and the force vector itself. The tangential and normal components of the acceleration can be therefore written as

$$\begin{cases} f_t = \dfrac{T}{m}\cos\phi \\ f_n = \dfrac{T}{m}\sin\phi \end{cases} \tag{3}$$

where $\dfrac{T}{m}$ is the maximum acceleration available at the given time. Since $\dot{r}_a$ should be as large as possible at any time in order to maximize the final apogee, the magnitude of the acceleration is considered to be always the maximum available and the thrust angle ϕ is the only control variable.

Therefore, the law to maximize the rate of change of the apogee can be derived by finding the roots of

$$\frac{\partial \dot{r}_a}{\partial \phi} = 0 \quad \Rightarrow \quad 2a\left[\frac{av}{\mu}(1+e)+\frac{e+\cos\vartheta}{v}\right]\sin\phi + \frac{r}{v}\sin\vartheta\cos\phi = 0 \tag{4}$$

The optimal thrust angle ϕ^* is then given by

$$\tan\phi^* = -\frac{r}{2av}\frac{\sin\vartheta}{\dfrac{av}{\mu}(1+e)+\dfrac{e+\cos\vartheta}{v}} \tag{5}$$

Since $\tan^{-1}$ returns only values of $\phi \in \left[-\frac{\pi}{2}, \frac{\pi}{2}\right]$ and the root of Eq. (4) can represent either a maximum, minimum or saddle, a study on the second derivative should be performed. However, a simple numerical check is computationally fast enough, so that the computation of the second derivative can be avoided. Defining ϕ_1^* as the angle given by solving Eq. (5) and $\phi_2^* = \phi_1^* + \pi$, the optimal thrust angle ϕ^* is given by

$$\begin{aligned} &\text{if } \dot{r}_a\left(\phi_1^*\right) \le 0 \ \wedge \ \dot{r}_a\left(\phi_2^*\right) \le 0 \\ &\quad \text{no thrust} \\ &\text{else} \\ &\quad \phi^* \text{ s.t. } \dot{r}_a\left(\phi^*\right) = \max\left(\dot{r}_a\left(\phi_1^*\right), \dot{r}_a\left(\phi_2^*\right)\right) \\ &\text{end} \end{aligned} \tag{6}$$

Numerical optimization approach to raise the apogee. The numerical approach is based on the idea of applying thrust to the spacecraft in order to maximize both apogee and eccentricity of the final orbit. The resulting trajectory is then ideally rotated in order to match one of the Moon nodes at the final point. The start sequence is divided into a few thousand segments of equal length of about one hour. These segments are sequentially optimized using the Brent optimizer*. The only optimization parameter here is the angle of the (full) thrust vector, which is a single value since we accelerate in the plane without considering inclination.

The objective function J_{Moon} to maximize has been chosen as

$$J_{Moon} = e^{0.07}\left(1+e\right)a - P_{Moon} \tag{7}$$

where P_{Moon} is a penalty value introduced in order to avoid the violation of the minimum-Earth-distance constraint. This objective function has been chosen in order to maximize the apogee of the resulting orbit with a slight emphasis on eccentricity. Fewer segments or a different objective function resulted in less hyperbolic excess velocity v_∞ at the Moon node, which reduces our options at the GA.

Comparison between analytical and numerical results. A 200-day optimal trajectory from the departing LEO is taken into account for comparing the analytical and numerical approaches described in the previous sections. In order to be consistent, the trajectories obtained by applying both control laws are propagated in time by means of a Bulirsch-Stoer propagator, with relative tolerance set to 10^{-12} and absolute tolerance set to 10^{-14}. The solution of the numerical optimization approach has been verified against the propagation with a 1 km tolerance in position, 0.1 m/s tolerance in velocity and 10^{-6} relative tolerance for the spacecraft mass.

The final apogee radius obtained by means of numerical optimization is $r_a^{(N)} = 428{,}840$ km, while the final apogee radius obtained by means of the analytical law is $r_a^{(A)} = 413{,}395$ km. The final radius of apogee found by applying the analytical law is 3.6% lower than the one found via a

* "Brent optimizer", URL: https://commons.apache.org/proper/commons-math/apidocs/org/apache/commons/math3/optim/univariate/BrentOptimizer.html, accessed on Jan, 6th 2016.

numerical optimization. This demonstrates that the analytical law to raise the apogee derived above is locally optimal only.

Figure 7 shows the control law found with both the numerical optimization and the analytical law, while Figure 8 shows the 200-days transfer trajectories found through the numerical optimization and the analytical law to raise the apogee.

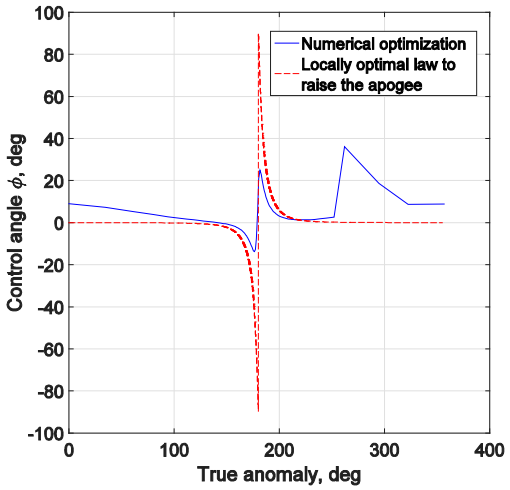

Figure 7. Control law (thrust angle over true anomaly) for the first complete revolution. Both the analytical law to raise the apogee (dotted red line) and the result of numerical optimization (continuous blue line) are shown.

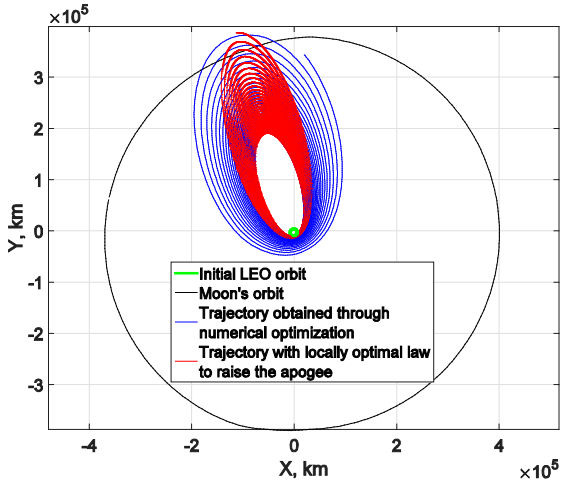

Figure 8. Earth-centered representation of the transfer trajectories obtained by applying the numerical optimal control law (blue) and the analytical control law (red).

Phasing

Since phasing of the starting spacecraft in the initial Earth orbit is fixed, an adjustment of the flight time (smaller than the period of the initial orbit) is required to reach the Moon node at the correct time. We performed a Covariance Matrix Adaptation Evolution Strategy (CMA-ES) optimization of the last 120 thrust vectors with two objectives: hit the Moon at the correct time and with the required norm of the incoming v_∞.

Sensitivity of Solutions and Golf-Hole Structure of the Search Space

In this context we detected that thrust can change the path of the perpendicular in a way that analyzing it deeply is not worth the time, as shown in Figure 2 and Figure 3. We found hard to predict the final value of an initial formation after GA, and the combinatorial landscape of the search space exhibits “golf-hole” behavior. That is, in the search space the objective function is very flat, and global minima (the golf holes) have only very small catchment areas[17]. An extreme example is a function with constant value 0 except for a single position x where the value is -1. Local search procedures have almost no chance to find this golf hole. So instead of spending much time on pre-evaluation of a single initial formation we chose a stochastic approach assessing a large number (about 10^{10}) very quickly, selecting only the very best for feeding the search. Since now we have the potential input velocity of the spacecraft at the two Moon nodes, we can generate randomly a huge number of valid starting formations and filter them in separate stages. This filtering and the whole search for sources are explained in detail in the following sub-section.

Search for sources

The search for sources works as follows (see Figure 9): given the potential input velocity v_∞ at the Moon node, a large number of initial formations (about 10^{10}) are randomly generated. The first filter stage checks for very high-valued sources potentially reachable in 15 days. That is, the orbits are propagated for 15 days with no thrust and the closest source to the perpendicular is considered for the first *J*-score evaluation. Only those formations with $J \geq 1.2 \times 10^6$ km (about 0.001% of the total initial formations) are kept for the next stage. Therefore we apply a beam search of fixed breadth (up to 300.000 branches) using the relative score (*J*-score/time) as selection criteria. Since we never reached the fuel limit we simply neglect fuel consumption. Finally, a continuous-thrust conversion is carried out on the final outputs of the beam-search algorithm. It is worth noting that the whole process can easily be parallelized, and we used 40 parallel processes on 4 machines for this task.

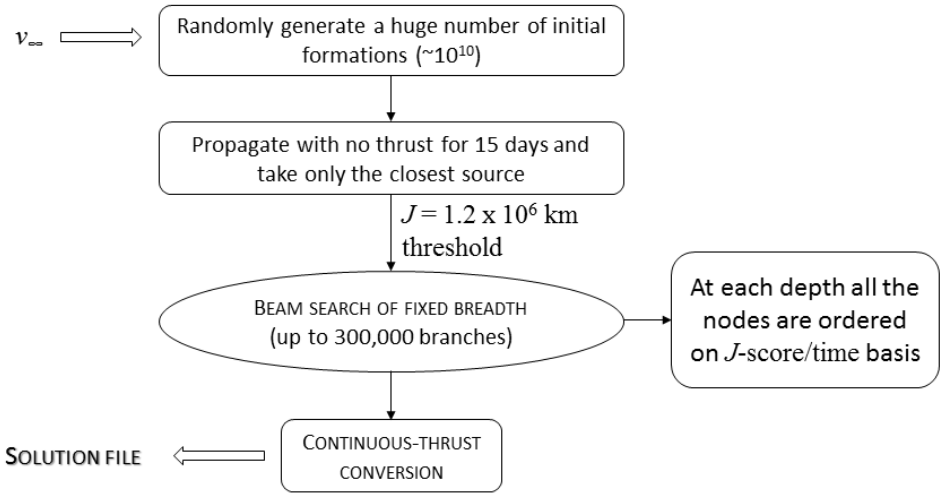

Figure 9. Flowchart of the search-for-sources algorithm.

We successfully applied this search approach to the tasks presented in previous competitions (GTOC4-7). For GTOC8 we observed that the high-score factors for repeated visits cause beam search to be guided in non-optimal directions, but the limited time did not allow us to develop a new algorithm. The beam-search algorithm, as used for the GTOC8, is as follow (see Figure 10).

Extension of the search nodes during search. For each search node, represented by a time and three (phased) spacecraft orbits, we can compute the perpendicular. We propagate the node without thrust by computing the perpendicular for a specific future time. For a node at time t_0 we compute all the nearest sources along the perpendicular path for t_0+15 days until t_0+25 days. For the best branches we slightly extend the maximal time to avoid losing these branches too early. Then we take the 15 target sources with the highest value of the score *J*, computed considering $P = 1$. We then check whether these are potentially reachable using a 1-DSM approach minimizing a function of the three thrust values and the resulting angular separation to the source. We applied BOBYQA for performing the aforementioned optimization, where the parameters of the optimization are all three thrust vectors and the target time.

We then filter the target sources reachable using a maximum thrust $T_{max} = 0.13$ N. These are further filtered using a 2-DSM approach keeping only sources with a very high probability of being reachable applying continuous thrust. In this way we avoid applying a continuous-thrust conversion during the search. Therefore, for target sources fulfilling the thrust limit by some margin we try to minimize the travel time further. Note that the same 2-DSM approximation was applied to the GTOC4 problem and resulted in a 46-point solution.

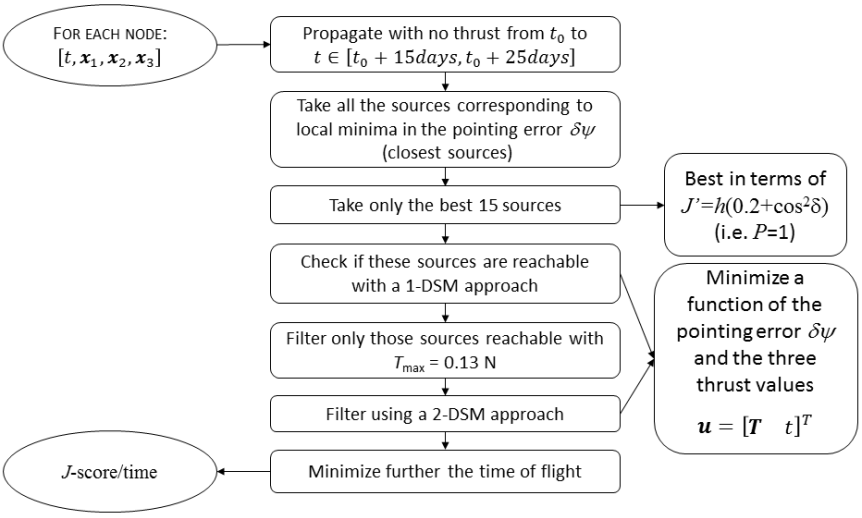

Figure 10. Flowchart of the beam-search algorithm.

Continuous-thrust conversion. After the search we compute continuous-thrust trajectories for the best branches. The conversion of the 2-DSM into continuous-thrust legs is performed within two steps. First a Sims-Flanagan approximation is performed segmenting the leg further into a *n*-DSM with $n \in [5, 13]$. Using a multi-threaded approach we assign different *n*-values to different threads. Thrust is minimized for this *n*-DSM applying CMA-ES. These *n*-DSM legs are used to build continuous-thrust legs with *n*+1 segments of equal length. For these legs we again apply CMA-ES to fulfil the constraints and minimize the continuous thrust.

Verification

The solution was verified to comply with the solution format specifications and constraints. Since the competition requires a very accurate solution, a significant amount of time has been dedicated to the verification phase. First, all the possible structures the solution file can look like have been investigated. Since we took into account only 1 Moon GA, this assumption has been made also in the search for possible structures within the solution file. It is worth to remind that each line of the solution file has the following entries:

TIME – POSITION – VELOCITY – MASS – THRUST

and that the first line of the solution file for each spacecraft must be the same. Since the mission starts when the first spacecraft begins to thrust, the first structure to be checked is related to the high-thrust (HT) burn. All the other possible structures are listed in Table 1.

Table 1. Details of all the possible structures that can be encountered within the solution file.

	Structure					Notes
	Time	Position	Velocity	Mass	Thrust	
HT burn	T1	P1	V1	M1	[0 0 0]	Just before HT
	T1	P1	V2	M2	[0 0 0]	Just after HT
HT – LT	T1	P1	V1	M1	[0 0 0]	Just after HT
	T1	P1	V1	M1	Thrust2	LT on
HT – coasting – LT	T1	P1	V1	M1	[0 0 0]	Just after HT
	T2	P2	V2	M1	[0 0 0]	End of coasting arc
	T2	P2	V2	M1	Thrust2	LT on
LT – coasting – LT	T1	P1	V1	M1	Thrust1	Last LT
	T1	P1	V1	M1	[0 0 0]	LT off – coasting arc begins
	T2	P2	V2	M1	[0 0 0]	Coasting arc ends
	T2	P2	V2	M1	Thrust2	LT on
LT – GA – LT	T1	P1	V1	M1	Thrust1	Last LT
	T1	P1	V1	M1	[0 0 0]	Just before GA
	T1	P1	V2	M1	[0 0 0]	Just after GA
	T1	P1	V2	M1	Thrust2	LT on again
LT – coasting – GA – LT	T1	P1	V1	M1	Thrust1	Last LT
	T1	P1	V1	M1	[0 0 0]	LT off – coasting arc begins
	T2	P2	V2	M1	[0 0 0]	Coasting arc ends – before GA
	T2	P2	V3	M1	[0 0 0]	Just after GA
	T2	P2	V3	M1	Thrust2	LT on again
LT – GA – coasting – LT	T1	P1	V1	M1	Thrust1	Last LT
	T1	P1	V1	M1	[0 0 0]	Just before GA
	T1	P1	V2	M1	[0 0 0]	After GA – coasting arc begins
	T2	P2	V3	M1	[0 0 0]	Coasting arc ends
	T2	P2	V3	M1	Thrust2	LT on again
LT – coasting – GA – coasting – LT	T1	P1	V1	M1	Thrust1	Last LT
	T1	P1	V1	M1	[0 0 0]	LT off – coasting arc begins
	T2	P2	V2	M1	[0 0 0]	Coasting arc ends – before GA
	T2	P2	V3	M1	[0 0 0]	After GA – coasting arc begins
	T3	P3	V4	M1	[0 0 0]	Coasting arc ends
	T3	P3	V4	M1	Thrust2	LT on again
End of the mission	T1	P1	V1	M1	Thrust1	Last LT
	T1	P1	V1	M1	[0 0 0]	LT off and mission ends

Once all the possible structures have been identified, the hypothesis made for the verification purpose are listed below.

1) Only 1 Moon GA.
2) Propagation with constant thrust in between two consecutive lines of the solution.
3) Propagation is restarted every approx. 3 revolutions.
4) Thrust set to zero for the HT burn.
5) Each spacecraft starts with either HT or coasting-HT.
6) Each spacecraft ends by switching off the LT (if any).
7) Propagation of the unperturbed Keplerian orbits are carried out via the approach described in Vallado [9].

Due to numerical accuracy of the optimization software employed, the following tolerances have been introduced within the verification phase, other than the ones given by the organizers and listed in the problem description.

$$\begin{cases} \text{Relative tolerance:} & 10^{-6} \\ \text{Threshold for zero thrust:} & 0 \text{ N} \\ \text{Threshold for maximum thrust:} & 10^{-8} \text{ N} \\ \text{Threshold for } \Delta v_{HT} \text{ to be consistent:} & 10^{-10} \text{ km/s} \\ \text{Threshold for mass after HT to be consistent:} & 10^{-10} \text{ kg} \end{cases} \tag{8}$$

All the steps used for the verification phase are as follow.

First of all, a check on the first line of the solution files for the three spacecraft is carried out in order to verify that these entries are exactly the same. Then, the solution file of each spacecraft is verified separately. The main points of the verification of each spacecraft's solution are listed below.

- Backward propagation of the state until $t_0 = 58849.0$ MJD, in order to check that the propagated state is the same as the initial one given in the problem description (within the relative tolerance of Eq. (8)).
- Check that the boundaries on magnitude of position vector, mass, initial and final time are satisfied during the whole mission.
- Check that the magnitude of LT is less than 0.1 N (within the 10^{-8} N tolerance of Eq. (8)). Moreover, all the times the magnitude of thrust is above 0.1 N but within the 10^{-8} N tolerance, the thrust vector is scaled so that the maximum thrust magnitude of 0.1 N is enforced.
- HT burn:
  - Check when the HT burn happens: it must be either in the first or second line of the solution file
  - If the HT burn is on line 2 (i.e. the current spacecraft is not the first one to thrust), propagate the Keplerian motion between line 1 and 2 and check the following:
    - Mass at line 2 must be the same as the propagated one.
    - Position and velocity at line 2 must be the same as the propagated ones (within the relative tolerance of Eq. (8)).
- Check the state after the HT burn:

  - Time and position before and after HT must be the same.
  - $\Delta v_{HT} \leq 3$ km/s (within the threshold given in Eq. (8)).
  - Mass after HT must be the same as the one computed via Tsiolkowski equation.
- Check the structure immediately after HT. It must be one of the following, as shown in Table 1 (note that a phase is considered as a coasting phase when the thrust is exactly zero):
  - HT-LT (i.e. LT immediately after the HT burn).
  - HT-coasting-LT.
- If the latter is a HT-LT structure, check that time and state (i.e. position, velocity and mass) at the line where the LT is turned on (LT-on phase) are the same as the ones listed in the line above.
- If the structure immediately after HT is a HT-coasting-LT structure, check the coasting phase first, and then the LT-on phase:
  - Coasting phase:
    - Position and velocity of the propagated unperturbed Keplerian orbit must be the same as the one listed in the solution file (within the relative tolerance of Eq. (8)).
    - Mass at the end of the coasting arc must be the same as the one at the beginning.
  - LT-on phase:
    - Time and state at LT on and before must be the same.
- Check on the final structure; it must be one of the following:
  - LT-end (the mission ends thrusting).
  - LT-coasting-end (the mission ends with a coasting phase).
- If thrust of i^{th} line of the solution file is zero, the following pseudo-code summarizes the checks carried out in order to understand what this line refers to:
  - If $\text{thrust}(i-1) \neq 0$, then line (i-1) is the last line of the current thrust-arc phase.
  - If $\text{thrust}(i+1) \neq 0$, then line (i+1) is the first line of the new thrust-arc phase.
  - If $\text{thrust}(i-1) \neq 0 \ \wedge \ \text{thrust}(i+1) \neq 0$, then there is an error in the solution file.
  - If $\text{thrust}(i+1)=0 \ \wedge \ \text{time}(i)=\text{time}(i+1)$, then lines (i) and (i+1) represent the Moon GA.
  - If $\text{thrust}(i+1)=0 \ \wedge \ \text{time}(i) \neq \text{time}(i+1)$, then lines (i) and (i+1) represent the initial and final time of a coasting-arc phase, respectively.
- For all the coasting arcs, the state at the beginning of the coasting arc is propagated forward in time for the whole duration of the arc. Therefore, position, velocity and mass of the propagated unperturbed Keplerian orbit are checked to be the same as the ones listed in the file (within the relative tolerance in Eq. (8)).
- Moon GA:
  - The constraints given by the organizers must be satisfied.
  - The mass before the Moon GA must be the same as the one after.
- LT arcs:
  - The state at the LT-on line of the solution file must be the same as the one listed in the line above of the solution file.
  - The state at the LT-off line of the solution file must be the same as the one listed in the line below of the solution file.

- Check the angular separation between two consecutive lines: it must be between 0.1 deg and 1 deg.
- Propagate the trajectory using a variable order Adam-Bashford-Moulton PECE solver (as implemented in MATLAB *ode113*) with absolute and relative tolerances set to 10^{-10}. The propagation is restarted after three full revolutions (and then rounded to the closer line in the solution file). The thrust is considered constant in between two consecutive lines of the solution file.
- Time, position, velocity and mass after each propagation must be the same as the ones in the trajectory file (within the relative tolerance in Eq. (8)).

The solution file has been then verified to comply with the solution format specifications. The solution file provides lines with a minimum angular separation of 0.14 deg and a maximum angular separation of 0.75 deg. The verification process validated our solution within the tolerances listed in Eq. (8). However, we are aware of the following (extremely small) violations of the constraints. We think these do not affect the validity of the solution.

- Maximum low-thrust violation of the upper limit of 0.1 N less than 2.7×10^{-17} N. However, we have verified through propagation that if the maximum thrust of 0.1 N is enforced (by rescaling the thrust vector magnitude whenever it exceeds 0.1 N), the tolerances on the state are not violated after 3 revolutions.
- The impulsive Δv_{HT} is close to 3 km/s within 3.6×10^{-15} km/s.
- The mass change over the impulsive maneuver is accurate to 1.36×10^{-12} kg.

DESCRIPTION OF SOLUTION

Our final solution has a performance index of $J = 5.97\times10^{7}$ km. The number of distinct sources observed is 27, and the sum of the final masses of the three spacecraft is 5846.57 kg. Table 2 provides an overview of our solution's figures of merit and characteristics, and Table 3 lists all the observations.

Each spacecraft starts its journey with a high-thrust impulse at the departing LEO, injecting into an elliptic orbit. After that, the low-thrust propulsion is used to raise the apogee until the Moon is encountered for a GA maneuver. Following the GA, the three spacecraft keep maneuvering using the low thrust, while targeting the radio sources.

The solution starts at 58863.41 MJD, when spacecraft 2 uses the full 3 km/s impulse followed by low thrust to reach the descending node of the Moon after about 285 days with an incoming v_∞ of approx. 1.184 m/s.

The other spacecraft start later, heading for the ascending node. We soon found out that it is worth the additional time you need for high v_∞ at the Moon to score higher after the GA. After the first and third spacecraft have performed their GA – the second is half a period earlier at the Moon – the formation starts to hunt for sources following the result of our search algorithm.

Table 2. Summary of solution.

Performance index J (km)	5.97×10^{7}
Number of observations	40
Number of unique observed sources	27
S/C 1 final mass (kg)	1949.84
S/C 2 final mass (kg)	1936.98
S/C 3 final mass (kg)	1959.76
Sum of final masses (kg)	5846.57
Start date (MJD)	58863.41
Total duration (days)	1086.56

Table 3. Radio sources observed (values of *h* and *J* rounded).

ID	*P*	*h* (km)	Cumulative Score *J* (km)	ID	*P*	*h* (km)	Cumulative Score *J*(km)
221	1	1200103	1437594	**171**	1	215557	30643593
188	1	211242	1682774	**334**	1	687829	31184386
166	1	959108	2811410	**171**	3	932856	34429651
187	1	1055511	4051199	**205**	1	204891	34675473
202	1	1043437	5302419	**205**	3	1051051	38458543
188	3	824752	8174196	**294**	1	474356	38898730
204	1	182115	8392733	**273**	1	186845	39099414
204	3	969986	11884673	**273**	3	931349	42100410
222	1	787151	12828877	**293**	1	517011	42665729
221	3	399030	14262861	**137**	1	218942	42909674
168	1	1135071	15589208	**137**	3	1044413	46400744
197	1	295520	15943746	**206**	1	323132	46788116
257	1	1237815	17386727	**206**	3	999326	50382101
170	1	232228	17656349	**325**	1	463368	50764876
170	3	1161601	21702300	**186**	1	183821	50977644
223	1	185786	21925207	**186**	3	874836	54015432
223	3	1044692	25685481	**295**	1	897305	54825401
258	1	744083	26546884	**259**	1	318361	55199332
185	1	332844	26930681	**259**	3	1142683	59225749
185	3	1001068	30393629	**77**	1	552255	59682715

The following sub-sections show trajectory, control and mass history of each of the spacecraft. The spacecraft trajectories are plotted in the physical space, projected on various planes for ease of visualization. Figure 10, Figure 13, and Figure 16 show the thrust histories of the three spacecraft. The saturation of the thrust at the beginning of the mission is visible, due to the fact that the three spacecraft must encounter the Moon as soon as possible, in order to have more time for the source-hunting phase.

Spacecraft 1

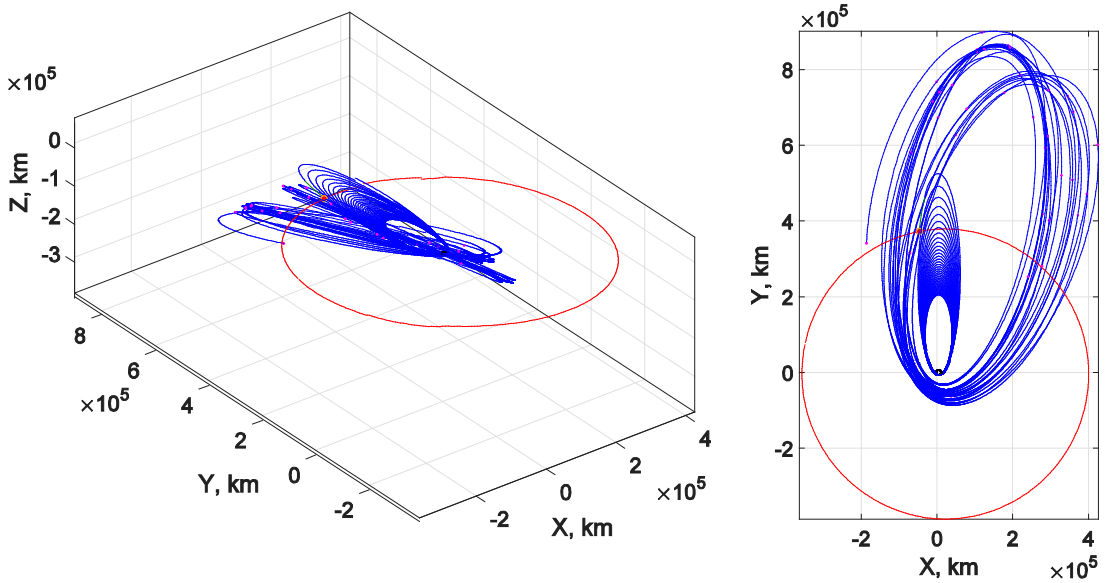

Figure 11. Spacecraft 1 trajectory (blue: thrusting arcs; green: coasting arcs). Moon orbit and GA in red. Observation points in magenta.

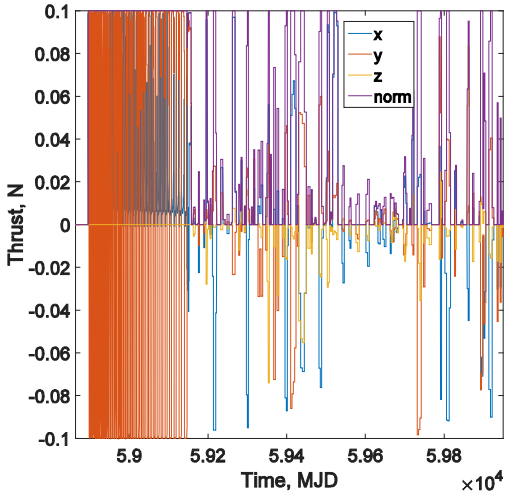

Figure 12. Spacecraft 1 thrust.

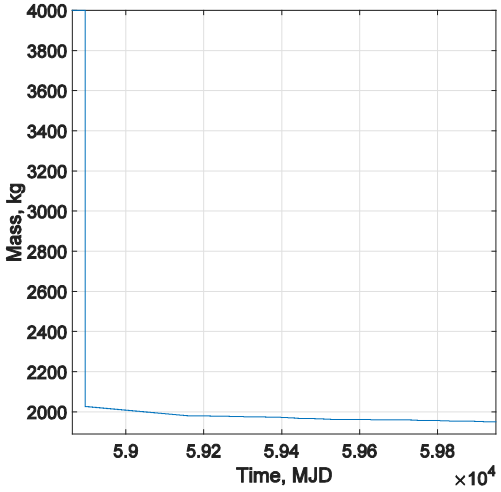

Figure 13. Spacecraft 1 mass.

Spacecraft 2

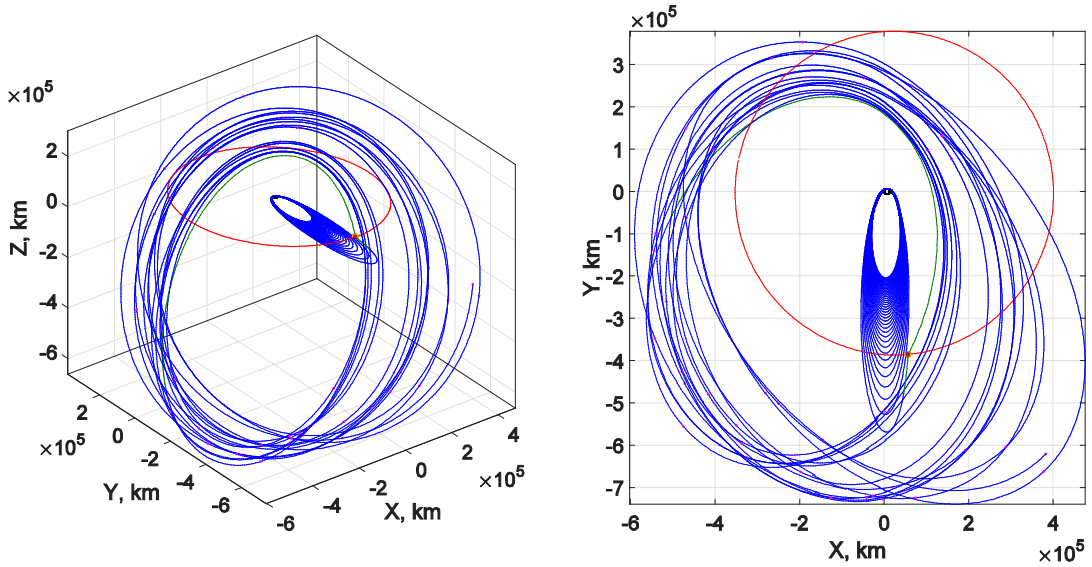

Figure 14. Spacecraft 2 trajectory (blue: thrusting arcs; green: coasting arcs). Moon orbit and GA in red. Observation points in magenta.

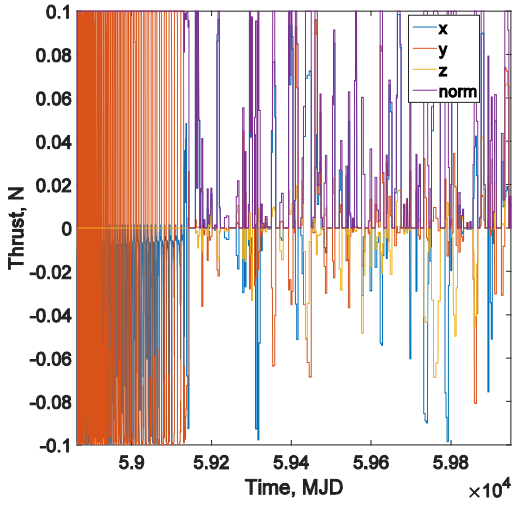

Figure 15. Spacecraft 2 thrust.

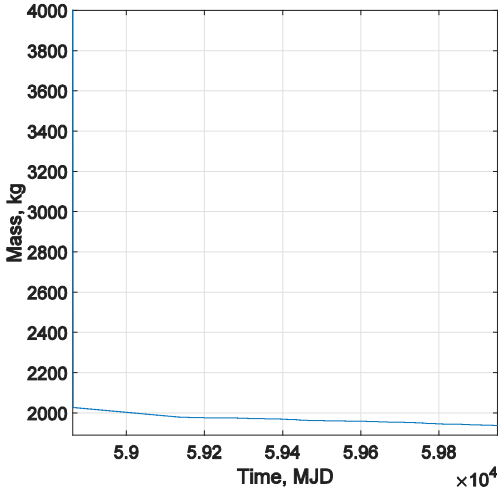

Figure 16. Spacecraft 2 mass.

Spacecraft 3

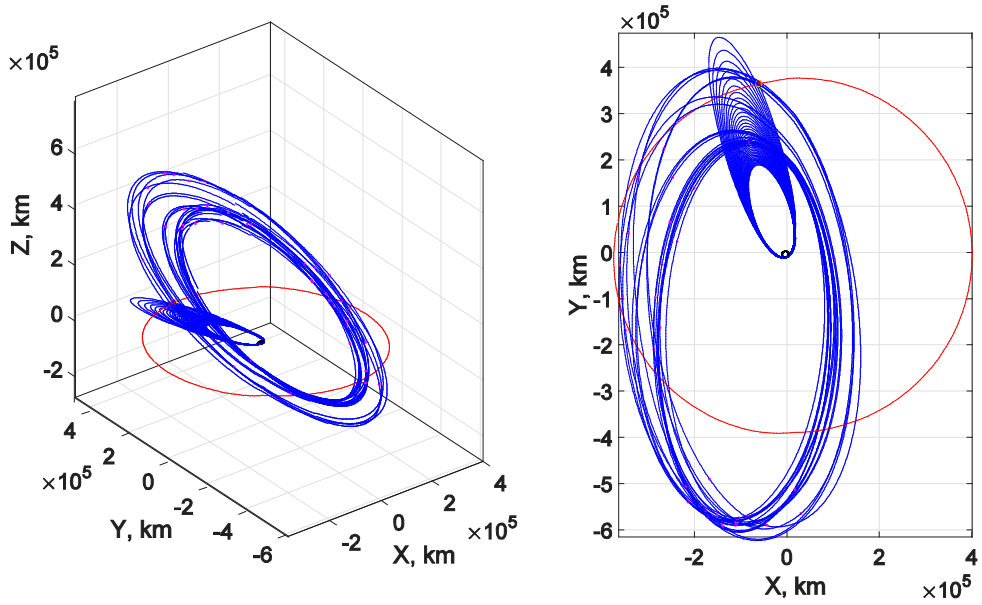

Figure 17. Spacecraft 3 trajectory (blue: thrusting arcs; green: coasting arcs). Moon orbit and GA in red. Observation points in magenta.

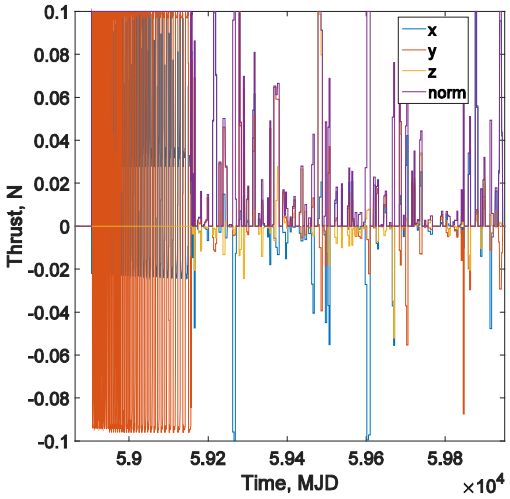

Figure 18. Spacecraft 3 thrust.

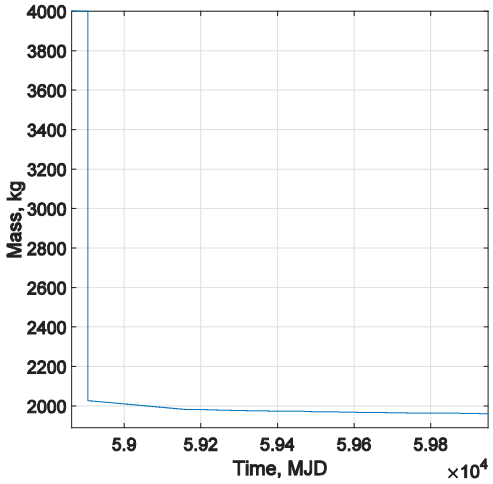

Figure 19. Spacecraft 3 mass.

Overall trajectory

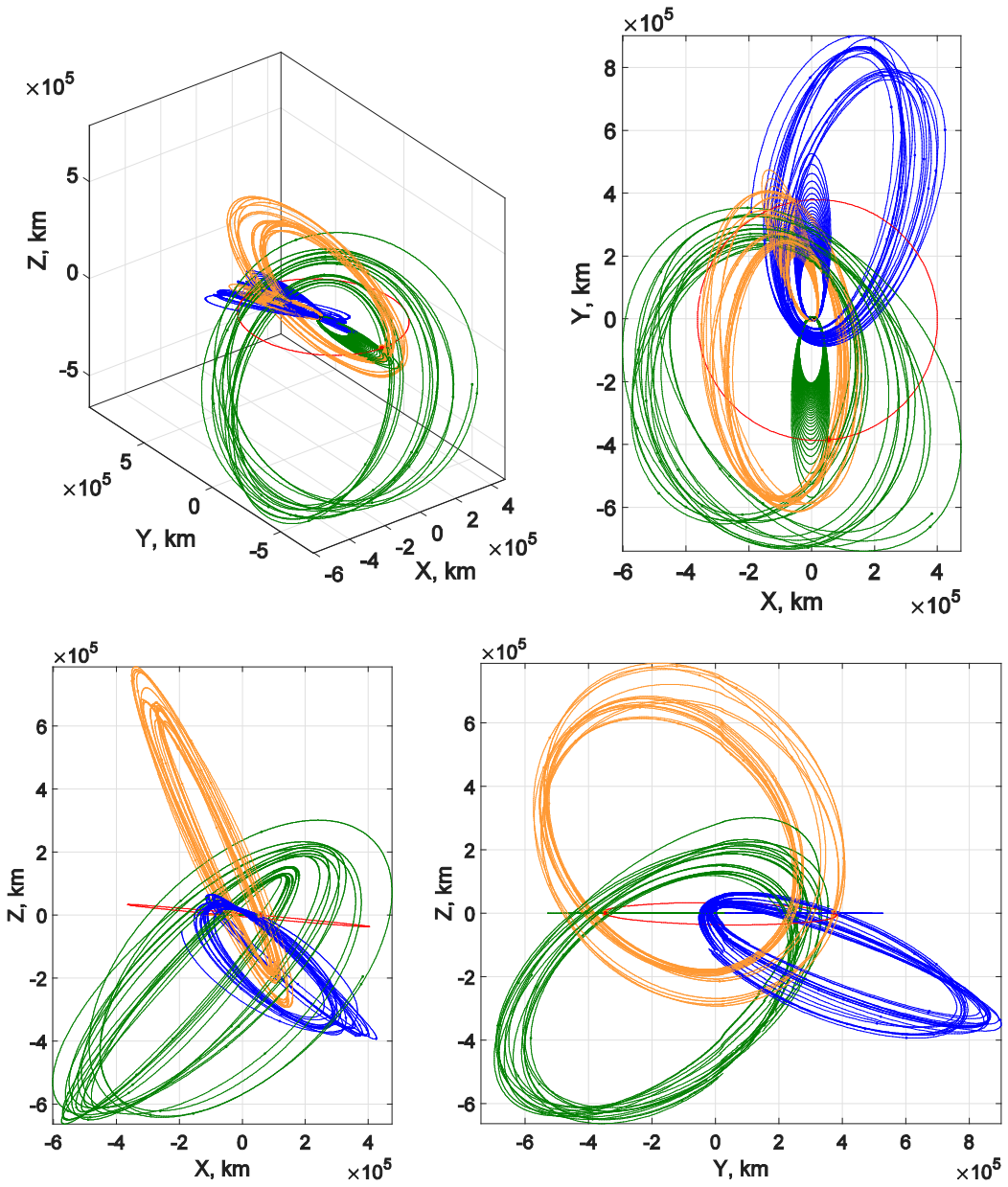

Figure 20. Overall spacecraft trajectories. Spacecraft 1: blue; Spacecraft 2: green; Spacecraft 3: yellow. Moon orbit and GAs in red.

CONCLUSIONS

In this paper we described the solution of the 8th Global Trajectory Optimization Competition problem, developed by Team 13, GlasgowJena+. Our solution is characterized by only one Moon Gravity Assist (GA) at the beginning of the mission. This allowed the three spacecraft to reach high-inclined orbits and therefore span a wide area in the α–δ space. However, the low-thrust itself was not able to drastically change the trajectories after the Moon GA. In fact, we have seen search results with $P = 6$, but our best trajectory only uses $P = 3$ in combination with high h values. We

found out that using high search breadth (>= 40,000) the search could very aggressively violate the maximum distance of 10^6 km to the Earth. This way we lost a trajectory scoring above 6×10^7 km, which fulfilled all the other constraints.

We also found many other solutions with $J > 5.5\times10^7$ km. If one ship could start a few periods earlier, even $J = 6.5\times10^7$ km is possible, as we found out during a search with a buggy code. Like in evolution with its central element of errors/mutations, a certain amount of errors also helps in the solution process of difficult optimization problems. Finally, we found that even a potential *J*-score of 7.5×10^7 km is possible when starting from a retrograde orbit around the Earth, leading to a much higher v_∞ about 1.8 km/s at the Moon.

Great effort was devoted to the verification process, because of the strict requirements of the competition. We already started our verification process in the early stages of the competition, and this led us to find and fix bugs in the code that were leading to wrong search paths. We can conclude that the verification process is not only useful to fulfill within the required tolerances, but it is a fundamental phase of the optimization process itself. It is important, therefore, to dedicate enough effort to the validation of the results not only during the last stage of the competition.

ACKNOWLEDGMENTS

We wish to thank Anastassios Petropoulos (Outer Planet Mission Analysis Group, Mission Design and Navigation Section, Jet Propulsion Laboratory, California Institute of Technology, CA, USA) for giving us the opportunity to work on this exciting and stimulating problem.

REFERENCES

[1] Petropoulos, A., "GTOC8: Problem Description and Summary of the Results", *26th AAS/AIAA Space Flight Mechanics Meeting*, Napa, CA, 2016.

[2] Gatto, G. and Casalino, L., "Fast Evaluation and Optimization of Low-Thrust Transfers to Multiple Targets", *Journal of Guidance, Control, and Dynamics*, Vol. 38, No. 8, 2015, pp. 1525-1530. doi: 10.2514/1.g001116

[3] Izzo, D., Hennes, D., Simões, L. F. and Märtens, M., "Designing Complex Interplanetary Trajectories for the Global Trajectory Optimization Competitions", *ArXiv e-prints*, 2015.

[4] Wall, B. J. and Conway, B. A., "Shape-based approach to low-thrust rendezvous trajectory design", *Journal of Guidance, Control, and Dynamics*, Vol. 32, No. 1, 2009, pp. 95-102. doi: 10.2514/1.36848

[5] Sims, J. A. and Flanagan, S. N., "Preliminary Design of Low-Thrust Interplanetary Missions", *AAS/AIAA Astrodynamic Specialist Conference*, Girdwood, Alaska, USA, 1999.

[6] Peloni, A., Ceriotti, M. and Dachwald, B., "Preliminary Trajectory Design of a Multiple NEO Rendezvous Mission Through Solar Sailing", *65th International Astronautical Congress*, International Astronautical Federation, Toronto, Canada, 2014.

[7] Grigoriev, I. S. and Zapletin, M. P., "Problem Description for the 5th Global Trajectory Optimization Competition", 2010, http://www.esa.int/gsp/ACT/doc/MAD/ACT-RPT-MAD-GTOC5-problem_stmt.pdf.

[8] Casalino, L. and Colasurdo, G., "Problem Description for the 7th Global Trajectory Optimisation Competition", 2014, 20/05/2014 - 17/06/2014, http://areeweb.polito.it/gtoc/gtoc7_problem.pdf.

[9] Vallado, D. A. and McClain, W. D., *Fundamentals of Astrodynamics and Applications, Second Edition*, Springer Netherlands, 2001, p.^pp. 101-102.

[10] Izzo, D., "Revisiting Lambert's problem", *Celestial Mechanics and Dynamical Astronomy*, Vol. 121, No. 1, 2015, pp. 1-15. doi: 10.1007/s10569-014-9587-y

[11] Powell, M. J. D., "The BOBYQA algorithm for bound constrained optimization without derivatives", University of Cambridge, DAMTP 2009/NA06, http://mat.uc.pt/~zhang/software.html.

[12] Arnold, D. V. and Hansen, N., "Active Covariance Matrix Adaptation for the (1+1)-CMA-ES", *Genetic And Evolutionary Computation Conference*, Portland, United States, 2010, pp. 385-392.doi: 10.1145/1830483.1830556

[13] Auger, A., Brockhoff, D. and Hansen, N., "Mirrored sampling in evolution strategies with weighted recombination", *Proceedings of the 13th annual conference on Genetic and evolutionary computation*, ACM, Dublin, Ireland, 2011, pp. 861-868.

[14] Pontani, M. and Conway, B. A., "Particle Swarm Optimization Applied to Space Trajectories", *Journal of Guidance, Control, and Dynamics*, Vol. 33, No. 5, 2010, pp. 1429-1441. doi: 10.2514/1.48475

[15] Ceriotti, M. and McInnes, C. R., "Design of ballistic three-body trajectories for continuous polar earth observation in the Earth–Moon system", *Acta Astronautica*, Vol. 102, No. 0, 2014, pp. 178-189. doi: 10.1016/j.actaastro.2014.06.001

[16] Battin, R. H., *An Introduction to the Mathematics and Methods of Astrodynamics*, Reston, VA, 1999, p.^pp. 492-493.

[17] Bernasconi, J., "Low autocorrelation binary sequences : statistical mechanics and configuration space analysis", *J. Phys. France*, Vol. 48, No. 4, 1987, pp. 559-567.